Investigation of Radiation Gain Enhancement Techniques for Microstrip Patch Antenna in Multilayer Superstrates

Michael F. Adamson[1,2], Ivor L. Morrow[2]
[1]DSTL, Porton Down, Salisbury, Wiltshire SP4 0JQ.
[2]EWIC, Cranfield University, Bedfordshire, MK43 0TR.

Abstract

An analytical method is described that gives insight into the behaviour of a microstrip patch antenna covered by planar dielectric and magnetic superstrates that allows significant gain improvements to be designed. Derived expressions for the TM_{01} mode electric field are combined with a transmission line model of the multilayer antenna structure to investigate the effect of key antenna design parameters such as superstrate permittivity and permeability, as well as air gaps between superstrate layers, on antenna radiation pattern and gain. Improvements in boresight gain up to 65.8dB is demonstrated and that superstrates that quarter wavelength thick superstrates give less gain than those that are thinner. Fast and flexible analytical tools provide useful alternatives to more expensive and complex full wave methods and especially for early stages of design optimization.

I. Introduction

A previous paper by the authors [1] described a computational electromagnetic and characteristic mode analysis study of a 10GHz microstrip patch antenna (MSA), in which planar dielectric superstrates were introduced to enhance the radiation pattern gain. A traditional cavity mode model was used to determine the initial resonance and impedance bandwidth for a MSA. Several multiple stacked planar superstrates were simulated using CST Microwave Studio and several prototype antenna system were manufactured, of the general form shown in Figure 1, and laboratory measurements made on impedance bandwidth, dielectric superstrate height and radiation pattern for comparison with the analytical and simulated results. The measured results showed less boresight gain than simulations predicted and the main lobe of the double superstrate configuration radiation pattern shows a pronounced distortion in Figure 2 where a number of possible causes were considered including: interference caused by the MSA microstrip feed, defects in the polycarbonate superstrates and an incorrect design of the multilayer antenna structure.

It is well known that patch antenna radiation can be increased via the integration of a combination of dielectric and/or ferrite superstrates or planar sheets. Previously researchers have employed full-wave analysis methods to design and optimise the material choice, thickness and separation in these complicated structures[2]. This approach is unwieldy, providing limited understanding and often leads to time consuming redesign if material layers are changed.

Here we describe the development of an equivalent transmission line model (TLM) that includes the patch antenna and the radiation model for an arbitrary dielectric/ferrite cascaded structure. The TLM enables rapid evaluation and understanding of the various effects that material selection and layer spacing have on the resultant radiated field pattern of the radiating system. We describe a parametric investigation for a multilayer patch antenna operating at 10GHz. The effect of key design parameters on radiation pattern and boresight gain are quantified numerically and the effect of variation in the permittivity of the superstrate layer, the thickness of the superstrate layer(s), dimensions of the antenna, and air gaps are

studied. Analytical results illustrating these various effects are presented and some configurations of more practical use are highlighted for manufacture and subsequent laboratory measurement. The results of CST full wave simulations and laboratory measurements for prototype radiating antenna will be compared with the TLM results in the conference presentation.

II. Analysis of Patch Antenna and Cascaded Superstrate Structure

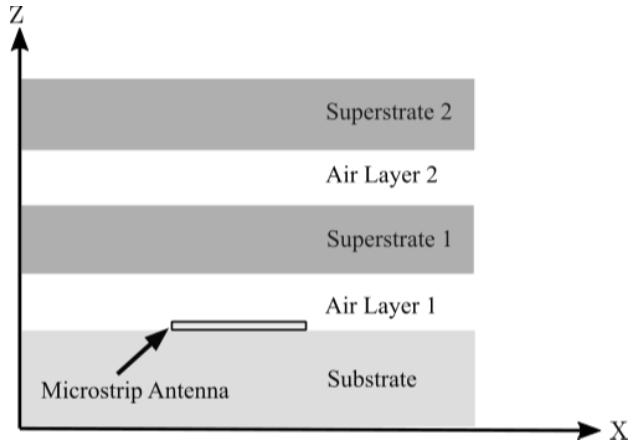

Fig. 1. A generalized configuration for the ABCD analysis of an MSA with superstrate and air layers

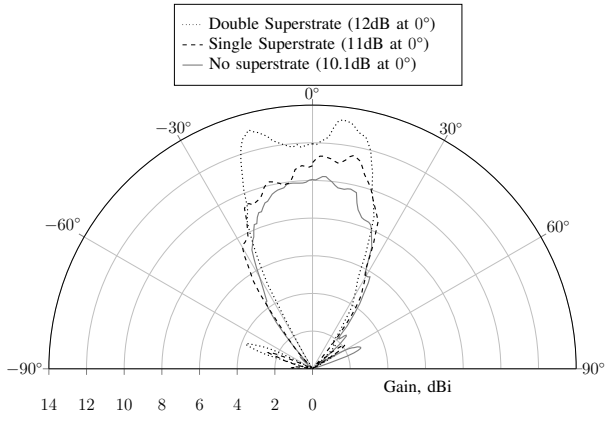

Fig. 2. E-plane radiation patterns for a patch antenna without and with single and double polycarbonate superstrates.

Intuitively, the modal current on the superstrate above the MSA should be a maximum for a maximum radiating field. This physically occurs when a single dielectric sheet is located approximately a quarter of guide wavelength $\frac{\lambda_g}{4}$ above the patch antenna resulting in a reinforcement of the radiated field. However the selection of the dielectric or ferrite materials and its thickness as well as the layer spacing must be fully taken into account. This situation becomes more complicated when multiple layers are considered.

A. Radiation form Microstrip Antenna

Figures 3 and 4 show a cavity model for the MSA and a coordinate system for computing the far field respectively. From the cavity model, the MSA at $z = h$ can be replaced by two magnetic current sources $\vec{M}_1$ and $\vec{M}_2$ along the y axis radiating an electric field of $\vec{E}_1$ and $\vec{E}_2$, respectively, at the observation point of $P(r, \theta, \phi)$.

The ground plane is accounted for by image theory which results in two $-\hat{a_y}$ directed magnetic dipole sources of strength $2\vec{E_0}$. Considering the two magnetic sources as radiating slots of width W and height h, they form a two element array separated by L, a $\frac{\lambda}{2}$ spacing. Auxiliary potential functions, $\vec{A_p}$ and $\vec{F_p}$ can be used to derive the electric and magnetic fields from the equivalent current density sources[3]. Since there is no $\vec{J}$ present $\vec{A_p} = 0$.

$$\vec{F_p} = \tfrac{\epsilon}{4\pi} \oint \vec{M} \frac{e^{-jkR}}{R} ds = \frac{\epsilon c}{4\pi r} L, \quad \text{where } L = \oint \vec{M} e^{jk(r' Cos\Psi)} \tag{1}$$

$r' Cos\Psi = r' \cdot \hat{a_r}$ in cartesian coordinates becomes $r' Cos\Psi = y' Sin\theta Sin\phi + z' Cos\theta$ in spherical coordinates. Now, the far field radiated electric field $\vec{E_\phi}$ is:

$$\vec{E_\phi} = \tfrac{jke^{-jkr}}{4\pi r}(L_\theta - \eta N_\phi), \quad \text{with no } \vec{J} \text{ there is no } N_\phi \text{ component and with substitution for } L_\theta \tag{2}$$

$$\vec{E_\phi} = \tfrac{jke^{-jkr}}{4\pi r}(-2\vec{E_0}) Cos\theta Sin\phi \left[\int_0^L \int_0^h e^{jk(y' Sin\theta Sin\phi + z' Cos\theta)} dz' dy' \right] \tag{3}$$

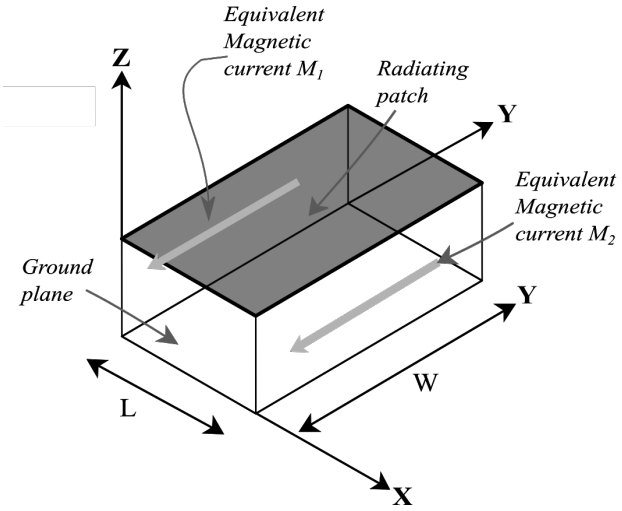

Fig. 3. Equivalent magnetic current sources, M_1 and M_2, representing the patch antenna.

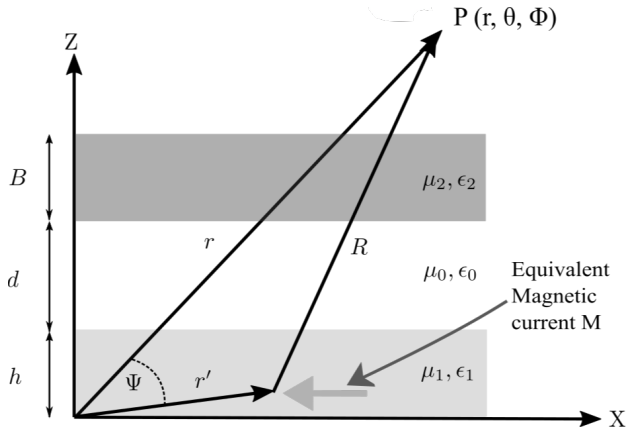

Fig. 4. Coordinate system for computing the far-field from the reciprocity electric source J2 at the patch antenna's radiation slot located at x = 0.

Equation 3 reduces to:

$$\vec{E_\phi} = \frac{jke^{-jkr}}{2\pi r} LV_0 Cos\theta Sin\phi \left[\frac{SinY}{Y}\right]\left[\frac{SinZ}{Z}\right] \text{ where } \quad Y = \frac{kL}{2} Sin\theta Sin\phi \text{ and } Z = \frac{kh}{2} Cos\theta \tag{4}$$

A similar derivation can be made for $\vec{E_\theta}$. The MSA can be analysed as a two element array where a general result for the Array Factor(AF) is:

$$AF_n = \frac{1}{N}\left[\frac{Sin\left(\frac{N\psi}{2}\right)}{Sin\left(\frac{\psi}{2}\right)}\right] \text{ and the particular case becomes } \quad AF = \frac{Sin\left(\pi Sin\theta Cos\phi\right)}{2Sin\left(\frac{\pi}{2} Sin\theta Cos\phi\right)} \tag{5}$$

Hence the total $\vec{E_\phi}$ and $\vec{E_\theta}$ fields due to both $\vec{M_1}$ and $\vec{M_2}$ for the dominant TM_{01} mode are:

$$\vec{E_\phi} = \frac{jke^{-jkr}}{4\pi r} LV_0 \left[Cos\theta Sin\phi \frac{SinY}{Y}\frac{SinZ}{Z}\right] \frac{Sin(\pi Sin\theta Cos\phi)}{2Sin\left(\frac{\pi}{2} Sin\theta Cos\phi\right)} \tag{6}$$

$$\vec{E_\theta} = \frac{-jke^{-jkr}}{4\pi r} \left[LV_0 Cos\phi \left[\frac{SinY}{Y}\right]\left[\frac{SinZ}{Z}\right]\right] \frac{Sin(\pi Sin\theta Cos\phi)}{2Sin\left(\frac{\pi}{2} Sin\theta Cos\phi\right)} \tag{7}$$

B. TLM Model of the Multilayer Microstrip Antenna Structure

As the E_θ and E_ϕ are plane waves, the effect on them from the antenna structure can be found by the transmission line analogy by assuming the air and superstrate layers are interconnected transmission line segments terminated by a short circuit, as depicted in Figure5. The refractive indices, $n_1(\theta)$ and $n_2(\theta)$, and the corresponding propagation constants, β_0, β_1, and β_2, related to the multi-section transmission line equivalent model are given by:

$$n_1(\theta) = \sqrt{n_1^2 - \sin^2\theta}, \quad n_2(\theta) = \sqrt{n_2^2 - \sin^2\theta}, \quad \eta_0 = \sqrt{\frac{\mu_0}{\epsilon_0}} \tag{8}$$

$$\beta_0 = K_0 \cos(\theta), \quad \beta_1 = K_0 n_1(\theta), \quad \beta_2 = K_0 n_2(\theta) \tag{9}$$

$$\tag{10}$$

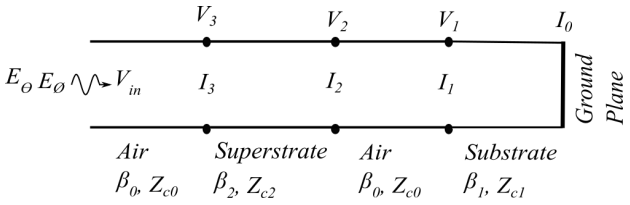

Fig. 5. Transmission line equivalent model of microstrip patch antenna with a superstrate cover.

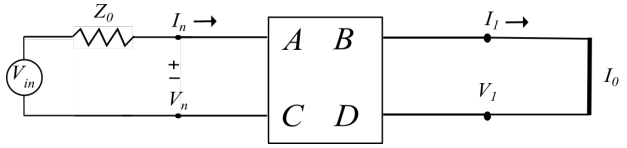

Fig. 6. Two port ABCD model.

The characteristic impedances for the TE wave or perpendicular polarization $Z_{c0_\perp}$, $Z_{c1_\perp}$, $Z_{c1_\perp}$ and the characteristic impedances for the TM wave or parallel polarization $Z_{c0_\parallel}$, $Z_{c1_\parallel}$, $Z_{c2_\parallel}$ are given by,

$$Z_{c0_\perp} = \eta_0 \sec(\theta), \quad Z_{c1_\perp} = \frac{\eta_0 \mu_1}{n_1(\theta)}, \quad Z_{c2_\perp} = \frac{\eta_0 \mu_2}{n_2(\theta)} \tag{11}$$

$$Z_{c0_\parallel} = \eta_0 \cos(\theta), \quad Z_{c1_\parallel} = \frac{\eta_0 n_1(\theta)}{\epsilon_1}, \quad Z_{c2_\parallel} = \frac{\eta_0 n_2(\theta)}{\epsilon_2} \tag{12}$$

A lossless transmission line is assumed and since the transmission line model of the MSA and superstrate structure is a series of four terminal networks connected in cascade, ABCD analysis can be used to characterize the system [4]. The ABCD matrix for the structure is the product of the individual ABCD matrices for each four terminal network. Equation 13 shows the general form ABCD matrix for a transmission line, where l is transmission line length between terminals and Z_0 is the transmission line characteristic impedance:

$$\begin{pmatrix} cos(\beta l) & jZ_0 sin(\beta l) \\ j\frac{1}{Z_0} sin(\beta l) & cos(\beta l) \end{pmatrix} \tag{13}$$

In the two port network shown in Figure 6 the following expressions can be stated,

$$\begin{bmatrix} 0 \\ I_0 \end{bmatrix} = \begin{bmatrix} A & B \\ C & D \end{bmatrix} \begin{bmatrix} V_n \\ I_n \end{bmatrix} \text{ , which gives: } 0 = AVn + BI_n \text{ and } I_0 = CV_n + DI_n \tag{14}$$

from which expressions for V_n, I_n and I_0 can be derived:

$$V_n = \frac{-BV_{in}}{(Z_0 A - B)} \tag{15}$$

$$I_n = \frac{AV_{in}}{(Z_0 A - B)} \tag{16}$$

$$I_0 = \frac{V_{in}}{(Z_0 A - B)} \quad \text{assuming a reciprocal network where } AD - BC = 1 \tag{17}$$

I_0 is the current flowing on the ground plane due to the far field radiation with V_{in} being either polarization E_θ or E_ϕ.

III. Results from ABCD Cascade Analysis

A parametric analysis of several multilayer configurations of the 10GHz MSA conforming to the generalized configuration shown in Figure 1 was performed where the effect of several factors on the antenna was examined. Insights from this examination were then used to optimize designs for increased boresight gain in this antenna structure.

A. Effect of Microstrip Antenna Width on Boresight Gain

The gain of a 10GHz MSA increases approximately linearly as the antenna width is increased as shown in Figure 12. This is explained by considering the cavity model where the distance between the two radiating elements of the MSA increases and so the AF increases and hence the gain will also increase.

B. Single Superstrate Configuration

The effect of changing the superstrate permittivity and thickness was investigated for a single superstrate suspended 1mm above a 10GHz MSA and the results in Figures 7 and 8 show very small increases in gain with thinner superstrates at higher permittivity.

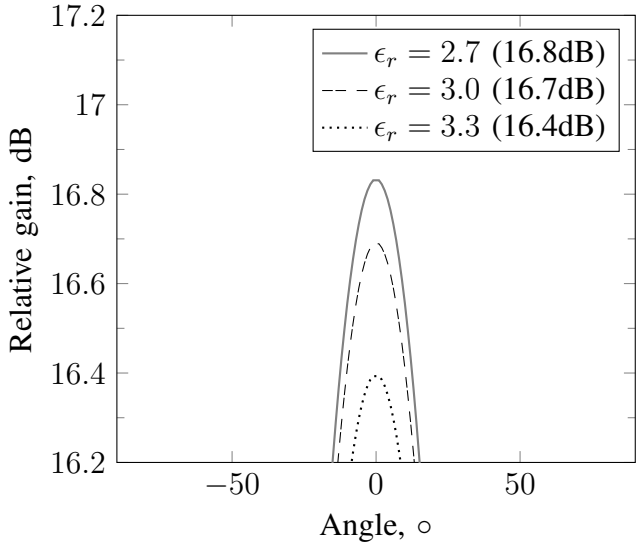

Fig. 7. ABCD calculated E-plane Gain of a 10GHz MSA with a 4.3mm thick single superstrate layer, with different permittivity, over a 1mm air layer

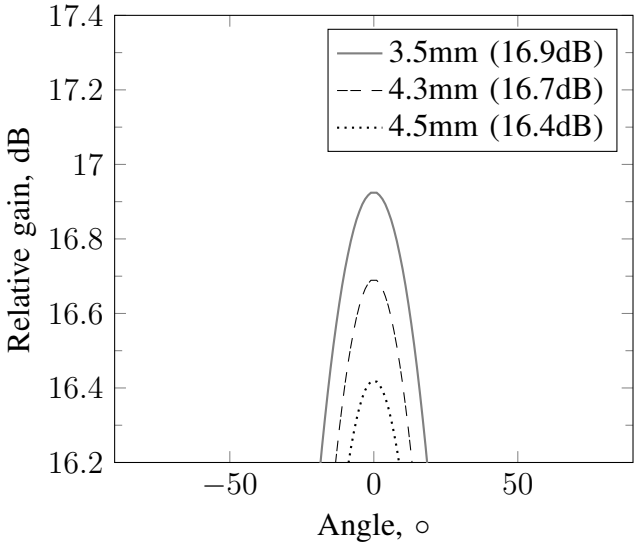

Fig. 8. ABCD calculated E-plane gain of a 10GHz MSA with a single $\epsilon_r = 3.0$ superstrate layer with varying superstrate thicknesses over a 1mm air layer.

Two types of Taconic [5] substrates, RF-30 with $\epsilon_r = 3$ and RF-10 with $\epsilon_r = 10$, were considered for analysis and using their standard production thicknesses of 0.25mm, 0.5mm, 0.76mm and 1.52mm for RF-30 and 0.25mm, 0.5mm, 0.64mm, 1.52mm and 3.18mm for RF-10 to further investigate the effect of permittivity and superstrate thickness on the 10GHz MSA. Figures 9 and 10 show that for each thickness of superstrate a resonance gain condition is achieved with a greater air gap as the superstrate becomes thinner for both RF-30 and RF-10. The gains for RF-30 and RF-10 are comparable for the same superstrate thickness where for example 0.5mm thick superstrates produce boresight gains of 22.7dB and 22dB for RF-30 and RF-10 respectively however the air gap needed for resonance is 64mm for RF-30 but only 44mm for RF-10 which would mean a more compact antenna structure for the same performance. An important point is that superstrates much less than a quarter wavelength give much better performance for gain enhancement than for the quarter wavelength case as shown in Figure 9 where the 4.3mm thick superstrate is the worst performing for RF-30.

Figure 11 summarizes the the effect of superstrate thickness on boresight gain and shows that the resonance gain for both RF-30 and RF-10 increases approximately linearly with a decrease in superstrate thickness and that for a single superstrate a lower permittivity gives higher boresight gain.

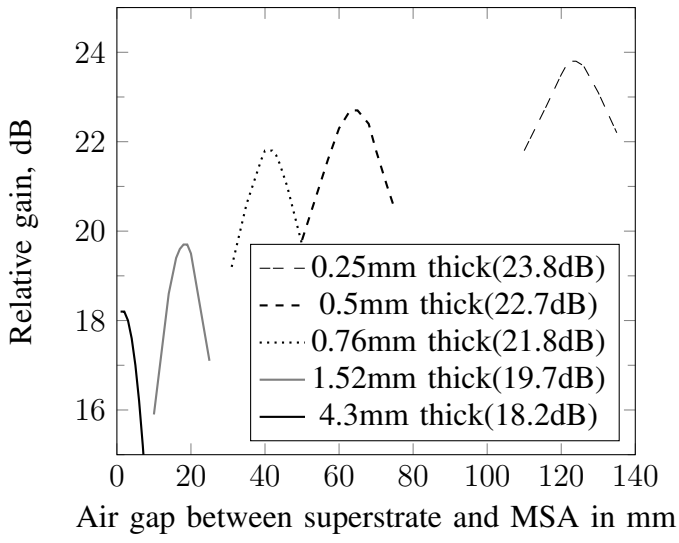

Fig. 9. ABCD cascade analysis of E-plane boresight gain for a 10GHz MSA with an $\epsilon_r = 3$ superstrate of four standard production thicknesses with different air gaps between the superstrate and MSA.

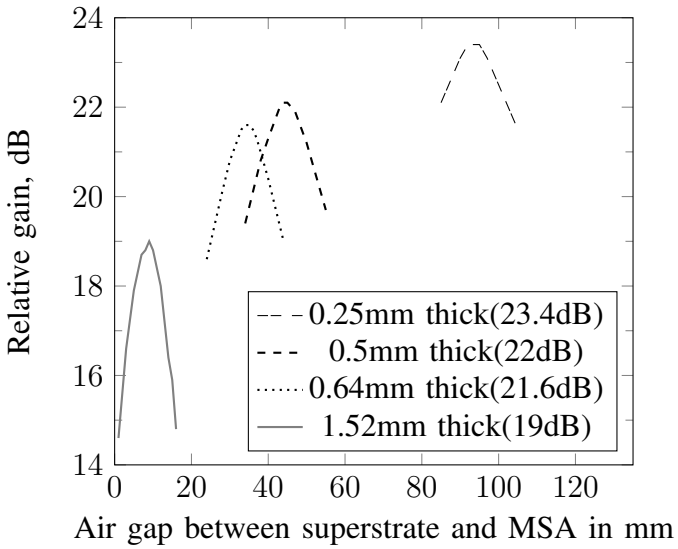

Fig. 10. ABCD cascade analysis of E-plane boresight gain for a 10GHz MSA with an $\epsilon_r = 10$ superstrate of five standard production thicknesses with different air gaps between the superstrate and MSA.

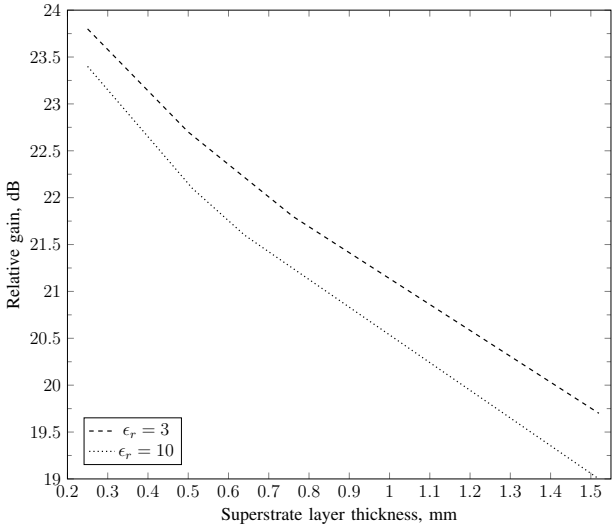

Fig. 11. ABCD cascade analysis of boresight resonance gain for varying superstrate thickness

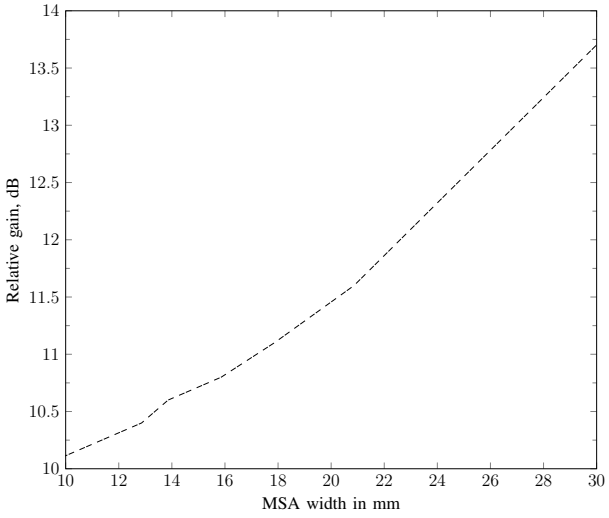

Fig. 12. ABCD cascade analysis of E-plane boresight gain of a 10GHz MSA with changing MSA width

C. Double Superstrate Configurations

Figure 13 shows the E-plane boresight gain of a 10GHz MSA when covered by a two-layer superstrate with no air layers comprising $\epsilon_r = 10$ and $\epsilon_r = 3$ for superstrate 1 and 2 respectively with each having several thicknesses of 0.25mm, 0.51mm, 0.64mm, 1.52mm, 3.18mm for superstrate 1 and 0.25mm, 0.5mm, 0.76mm and 1.52mm for superstrate 2. For 0.25mm, 0.51mm and 0.64mm thick superstrate 1 the gain increases by approximately 3dB per extra 1mm thickness of superstrate 2. As $\epsilon_r = 10$ becomes thicker the increase in gain is affected and for 1.52mm thick the gain decreases when superstrate 2,$\epsilon_r = 3$ is above 0.8mm thick. When $\epsilon_r = 10$ is 3.18mm the gain decreases for all thicknesses of $\epsilon_r = 3$. Figure 14 shows the opposite case where $\epsilon_r = 3$ is superstrate 1 and $\epsilon_r = 10$ is superstrate 2 and for all thicknesses

of superstrate layer 1 the gain has a peak particular to the thickness of superstrate layer 2 and the rise and fall in gain is 4.9dB per 1mm change in superstrate layer 2 thickness.

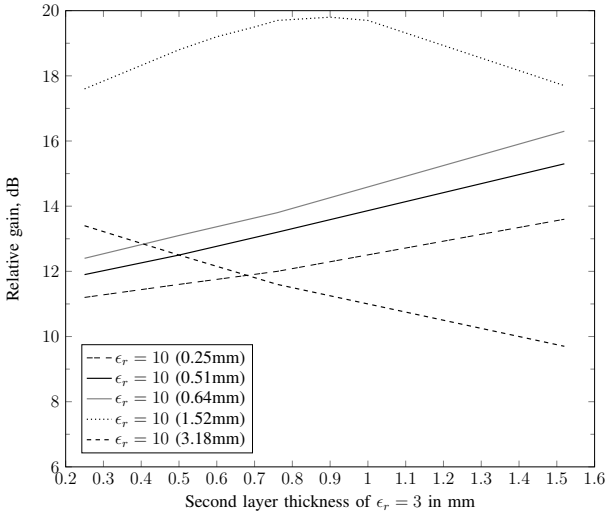

Fig. 13. ABCD cascade analysis of E-plane boresight gain for a 10GHz MSA with combinations of $\epsilon_r = 10$ superstrate of five standard production thicknesses of 0.25mm, 0.51mm, 0.64mm, 1.52mm and 3.18mm as a first layer with a second layer of $\epsilon_r = 3$ of four standard production thicknesses of 0.25mm, 0.5mm, 0.76mm and 1.52mm covering the MSA.

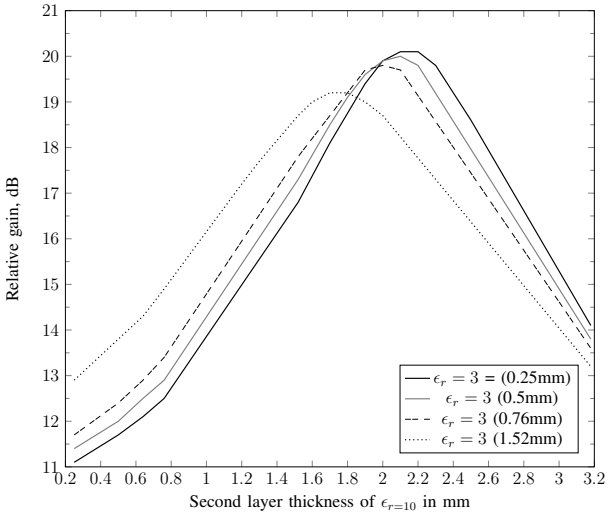

Fig. 14. ABCD cascade analysis of E-plane boresight gain for a 10GHz MSA with combinations of $\epsilon_r = 3$ superstrate of four standard production thicknesses of 0.25mm, 0.5mm, 0.76mm and 1.52mm as a first layer with a second layer of $\epsilon_r = 10$ of four standard production thicknesses of 0.25mm, 0.51mm, 0.64mm, 1.52mm and 3.18mm covering the MSA.

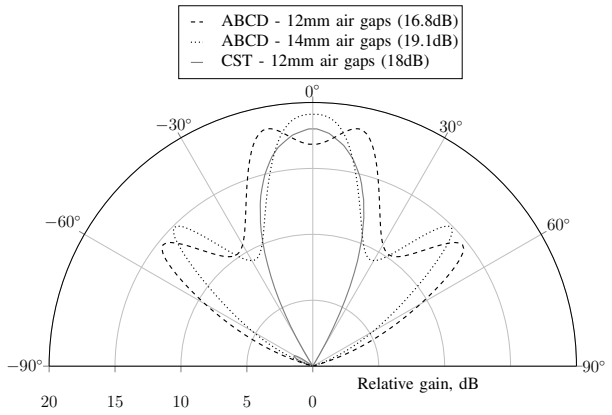

Fig. 15. Maximum E-plane gain of a 10GHz MSA with two 4.3mm thick, $\frac{\lambda_r}{4}$, superstrates of $\epsilon_r = 3$ where CST had 12mm air gaps and ABCD method had 14mm air gaps

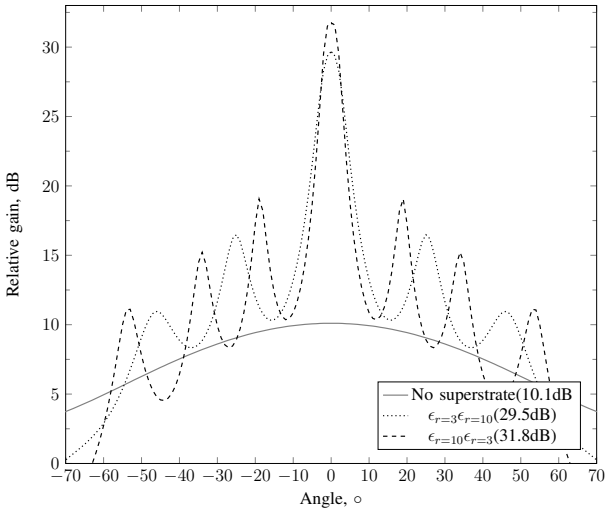

Fig. 16. 10GHz MSA resonance gain double superstrate configuration of a 0.5mm $\epsilon_{r=10}$ and $\epsilon_{r=3}$ superstrate in alternate superstrate 1 and 2 positions

Figure 15 shows the gain for a double superstrate configuration 10GHz MSA, illustrated in Figure 1, where each superstrate is $\epsilon_r = 3$ and electrically a quarter wavelength thick, $\frac{1}{4}\lambda_R$, at 4.3mm and this was the configuration used in the authors previous work [1]. This shows the sensitivity of the boresight maximum gain to a slight change in air layers where it is reduced from 19.1dB to 16.8dB with an air gaps just 2mm smaller for air layer 1 and 2. A maximum boresight gain of 18dB, calculated by CST, was realized with air layers 1 and 2 of 12mm and the similarity in gain between the full-wave and analytical

derivations provide a verification of the ABCD cascade analysis. The difference is due to the ABCD cascade analysis using an expression for just the TM_{01} mode of the electric field for the MSA. This result indicates that the air gaps need to be sufficiently large to allow a plane wave to be incident on the superstrate and which will give the greatest diffraction according to Snell's law resulting in the resonance gain. The ABCD cascade analysis allows iterative tuning of the air gaps to find the resonance gain.

The resonance gain of a double superstrate configurations was investigated comprising one RF-30 and one RF-10 superstrate and comparing the effect of having them alternately in superstrate 1 and 2 positions. Both superstrates were 0.5mm thick since this gives good gain with the mid-size air gaps for the single superstrate case as shown in Figures 10 and 9. The results in Figure 16 show that having RF-10 as a first superstrate layer with RF-30 above it, with air layer 1 and 2 of 0mm and 58mm respectively, gives the best boresight gain of 31.8dB and a total antenna height of 59mm and the configuration with the superstrate positions swapped, with air layer 1 and 2 of 0mm and 48mm respectively, giving 29.5dB. Both plots show that the inclusion of air layers means the antenna pattern shows increased sidelobes

D. Double Superstrate Configurations Incorporating Magnetic Superstrates

Figure 17 shows the effect on the boresight gain when various thicknesses of a superstrate of RF-10 are covered by a 4.3mm thick superstrate of $\mu_r = 4$ with no air layers.

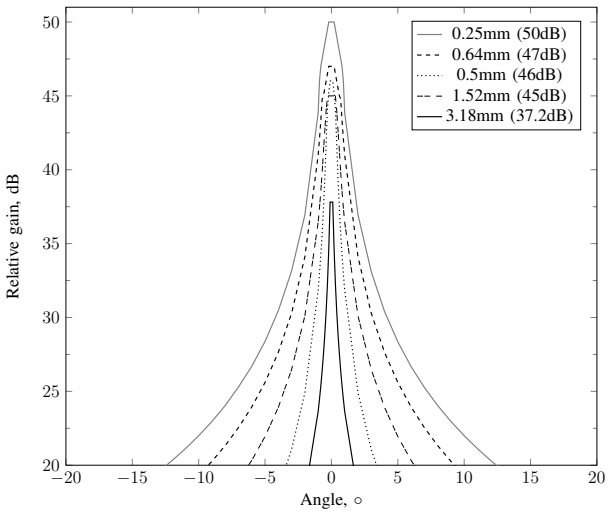

Fig. 17. 10GHz MSA resonance gain with a RF-10 superstrate of different thickness of 0.25mm, 0.51mm, 0.64mm, 1.52mm and 3.18mm as superstrate 1 and $\mu_r = 4$ of 4.3mm as superstrate layer 2

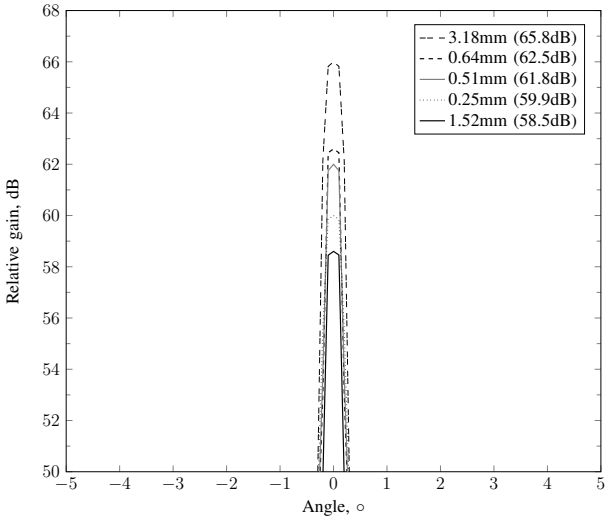

Fig. 18. 10GHz MSA resonance gain with RF-10 as superstrate 1 of different thickness of 0.25mm, 0.51mm, 0.64mm, 1.52mm and 3.18mm with 4.3mm thick $\mu_r = 4$ as superstrate 2 with air layers 1 and 2 of 0mm and 14mm respectively except for the configuration with 3.18mm thick superstrate 1 where air layer 1 was 29mm.

The highest gain of 50dB is achieved with a 0.25mm thick superstrate of RF-10 that gives a total structure height of 4.25mm. The gain reduces as RF-10 becomes thinner. The increased boresight gain from the inclusion of a magnetic superstrate as the top layer is due to the added gain it provides in the H plane. Adding air layer 1 and 2 of omm and 14mm respectively to the configuration further increases the gain as shown in Figure 18 where the highest gain of 65.8dB is achieved with superstrate layer 1 of RF-10 at 3.18mm thick. This makes the total height of the antenna structure 21.18mm. With the inclusion of a magnetic superstrate the gain is significantly increased and with no air layers the increased antenna height of 4.25mm for a gain of 50dB is the best performance overall. An example materials suitable as

a magnetic superstrate may be hexaferrites although the use of metamaterials may be a more pragmatic choice for a practical system.

IV. Conclusions

The effect of various parameters for a 10GHz MSA antenna structure comprising single and double supertrate configurations have been examined. Analysis using a TLM model comprising cascaded ABCD networks demonstrated the significance of a number of factors that produce significant boresight gain enhancements of up to 65.8dB. Beneficial increments in gain were feasible for single and double stacked superstrates of different permittivity and thickness as well as the inclusion of magnetic superstrates. Increasing the MSA width produces an almost linear increase in gain at the same MSA design frequency whilst a increasing superstrate permittivity gives slightly lower gain but this allows a much thinner air layer to be used for resonance gain.

A critical factor in producing a resonant gain condition is using a sufficiently large air layer between superstrates to allow the radiated wave from the MSA to appear plane at the last superstrate. This study has also shown that thick superstrates can cause diminished gain and particularly if a higher permittivity superstrate is the first layer. The cost is an increased height for the MSA, however, a magnetic superstrate demonstrates additional antenna heights of only 4.25mm for a gain of 50dB with no air layers. This also suggests that the use of metamaterials to further increase the design options and performance would be useful.

Incorrectly chosen air layer thicknesses has deleterious effects on both the radiation pattern and the boresight gain and this is the most likely cause of the poor performance of the antenna in the authors previous work [1]. The air layer thickness was compounded by using 4.3mm thick polycarbonate of $\epsilon_r = 3$ which is very flexible which may have resulted in perturbations of a few millimetres during measurement. An improved design would benefit from the increased rigidity of RF-30 and a thickness of 0.5mm would improve the gain.

The TLM model used in this study has demonstrated a valuable ability to quickly produce numerical information that gives insight into the antenna structure behaviour. This has enabled a systematic approach for antenna optimization to be investigated where the non-linearity of the total antenna system behaviour can be investigated by adjusting single factors to observe the action on individual system parts as well as the total system.

Acknowledgment

Michael Adamson acknowledges the support received for his studies from his employer, DSTL.

References

[1] M. F. Adamson, I. L. Morrow, and D. James, "Behaviour of Characteristic Modes on Patch Antennas in Multilayered Media," in *Autom. RF Microw. Meas. Soc.*, 2022, pp. 1–10.

[2] N. G. Alexópoulos and D. R. Jackson, "Fundamental Superstrate (Cover) Effects on Printed Circuit Antennas," *IEEE Trans. Antennas Propag.*, vol. 32, no. 8, pp. 807–816, 1984.

[3] C. A. Balanis, *Antenna Theory: Analysis and Design*, 3rd ed. Wiley Interscience, 2005.

[4] D. M. Pozar, *Microwave engineering*. Wiley, 2012.

[5] "Taconic RF Laminates." [Online]. Available: http://www.taconic.co.kr/english/pages/sub02{_}03.php